Journal of Hydraulic Research
Publication details, including instructions for authors and subscription information:
http://www.tandfonline.com/loi/tjhr20

# Three-phase bi-layer model for simulating mixed flows

Francois Kerger [a], Pierre Archambeau [b], Benjamin J. Dewals [c], Sébastien Erpicum [d] & Michel Pirotton [e]

[a] Hydrology, Applied Hydrodynamics and Hydraulic Constructions (HACH), ArGEnCo Department, MS²F Sector, University of Liège (ULg), Chemin des chevreuils, 1, bât B52/3, étage +1, 4000, Liège, Belgium

[b] Hydrology, Applied Hydrodynamics and Hydraulic Constructions (HACH), ArGEnCo Department, MS²F Sector, University of Liège (ULg), Chemin des chevreuils, 1, bât B52/3, étage +1, 4000, Liège, Belgium E-mail:

[c] Hydrology, Applied Hydrodynamics and Hydraulic Constructions (HACH), ArGEnCo Department, MS²F Sector, University of Liège (ULg), Chemin des chevreuils, 1, bât B52/3, étage +1, 4000, Liège, Belgium E-mail:

[d] Hydrology, Applied Hydrodynamics and Hydraulic Constructions (HACH), ArGEnCo Department, MS²F Sector, University of Liège (ULg), Chemin des chevreuils, 1, bât B52/3, étage +1, 4000, Liège, Belgium E-mail:

[e] Hydrology, Applied Hydrodynamics and Hydraulic Constructions (HACH), ArGEnCo Department, MS²F Sector, University of Liège (ULg), Chemin des chevreuils, 1, bât B52/3, étage +1, 4000, Liège, Belgium E-mail:

Version of record first published: 25 Jun 2012

To cite this article: Francois Kerger, Pierre Archambeau, Benjamin J. Dewals, Sébastien Erpicum & Michel Pirotton (2012): Three-phase bi-layer model for simulating mixed flows, Journal of Hydraulic Research, 50:3, 312-319

To link to this article: http://dx.doi.org/10.1080/00221686.2012.684454

*Journal of Hydraulic Research* Vol. 50, No. 3 (2012), pp. 312–319
http://dx.doi.org/10.1080/00221686.2012.684454


Research paper

# Three-phase bi-layer model for simulating mixed flows

FRANCOIS KERGER, FNRS-FRS Fellow, *Hydrology, Applied Hydrodynamics and Hydraulic Constructions (HACH), ArGEnCo Department, MS²F Sector, University of Liège (ULg), Chemin des chevreuils, 1, bât B52/3, étage +1, 4000 Liège, Belgium. Email: fkerger@alumni.ulg.ac.be (author for correspondence)*

PIERRE ARCHAMBEAU, Research Scientist, *Hydrology, Applied Hydrodynamics and Hydraulic Constructions (HACH), ArGEnCo Department, MS²F Sector, University of Liège (ULg), Chemin des chevreuils, 1, bât B52/3, étage +1, 4000 Liège, Belgium. Email: pierre.archambeau@ulg.ac.be*

BENJAMIN J. DEWALS, Research Scientist, *Hydrology, Applied Hydrodynamics and Hydraulic Constructions (HACH), ArGEnCo Department, MS²F Sector, University of Liège (ULg), Chemin des chevreuils, 1, bât B52/3, étage +1, 4000 Liège, Belgium. Email: b.dewals@ulg.ac.be*

SÉBASTIEN ERPICUM, Laboratory Manager, *Hydrology, Applied Hydrodynamics and Hydraulic Constructions (HACH), ArGEnCo Department, MS²F Sector, University of Liège (ULg), Chemin des chevreuils, 1, bât B52/3, étage +1, 4000 Liège, Belgium. Email: s.erpicum@ulg.ac.be*

MICHEL PIROTTON, Professor, *Hydrology, Applied Hydrodynamics and Hydraulic Constructions (HACH), ArGEnCo Department, MS²F Sector, University of Liège (ULg), Chemin des chevreuils, 1, bât B52/3, étage +1, 4000 Liège, Belgium. Email: michel.pirotton@ulg.ac.be*



**ABSTRACT**
Mixed flows characterized by a simultaneous occurrence of free surface and pressurized flows are often encountered in hydraulic engineering. Numerous researches have been dedicated to unify the mathematical description of both flows. Herein, shock-capturing models succeed in giving a unique set of equations. However, no method accounts for both air-entrapment and air-entrainment. This study proposes an original model to simulate air–water interactions in mixed flows. The new approach relies on the area-integration of a three-phase model over two layers. The applicability of this free surface model is extended to pressurized flows by a modified pressure term accounting for the dispersed air. The derived modelling system WOLF IMPack is then validated. The code successfully simulates open channel flows, mixed flows and water hammer in a unified framework, including air–water interactions, in structures like the drainage network.

*Keywords:* Air entrapment; air entrainment; air–water flow; drift-flux model; multiphase flow

## 1 Introduction

Accidents to existing sewer systems are reported by Guo and Song (1990, 1991), Zhou *et al.* (2002) or Vasconcelos and Wright (2009). These have important detrimental effects, notably causing structural damage to hydraulic structures and inducing uncontrolled floods and pollution. These phenomena are linked to an incorrect appreciation of three dynamic features, namely transient mechanisms affecting flows, mixed flows characterized by the simultaneous occurrence of free surface and pressurized flows, and the effect of air–water interactions (air-entrainment and air-entrapment).

Since the 1960s, mathematical and numerical models describing transient air–water mixed flows were developed. Two families of approaches succeeded to overcome the discrepancy between pressure gradients appearing in unsteady free surface and pressurized flows equations. First, the shock-tracking approach solves separately free-surface and pressurized flows (Guo and Song 1990). Li and McCorquodale (1999) proposed the rigid water column model by integrating the effect of air entrapment. It relies on a specific model for the air above the free surface, but neglects the compressibility of water in the pressurized portion. The second traditional approach for mixed flow simulations is the shock-capturing approach. The free surface

Revision received 10 April 2012/Open for discussion until 30 November 2012.

ISSN 0022-1686 print/ISSN 1814-2079 online
http://www.tandfonline.com

and pressurized flows are computed by means of a single set of equations. Only four models appear to fall into this category: the Preissmann slot and its improvements (Leon *et al.* 2008, Kerger *et al.* 2009), the two-component pressure approach (TPA) (Vasconcelos and Wright 2007), the dual model (Bourdarias and Gerbi 2008), and the kinetic model (Bourdarias *et al.* 2008). Further, only two references propose to integrate air–water interactions into a shock-capturing model. First, an overpressure term is added in the TPA model to account for the pressurization of the air pocket above the free surface (Vasconcelos *et al.* 2006). Leon *et al.* (2010) proposed similarly a two-equation model that adequately simulates the entrapment and release of air. They added equations describing steady free-surface flows by the ideal gas law. However, no model integrates the effect of both air-entrainment and air-entrapment in transient mixed flows. In addition, all shock-capturing models are known to develop post-transition oscillations (Politano *et al.* 2007, Leon *et al.* 2010). This problem is linked to the rapid variation of the pressure wave celerity at the transition (Vasconcelos *et al.* 2009). Herein, their artificial reduction of the pressure wave celerity and a numerical filter are used.

To simulate air-entrapment and air-entrainment in transient mixed flows, this research establishes an original bi-layer three-phase mathematical model (Section 2), which is then discretized to develop the original computational code WOLF IMPack (Section 3). In Section 4, the validity and applicability of this module are assessed by comparison with experimental, analytical, and numerical results.

## 2 Multiphase mathematical model

The use of multiphase models in hydraulic engineering has so far remained limited to only few attempts. A worthwhile example of ingenious application of these models to vaporous cavitation was proposed by Shu (2003). His two-phase homogeneous equilibrium model improves the conventional column separation model for cavitation. His results on the drift-flux model (Jha and Bombardelli 2009) prompt us to use multiphase models for describing air–water interactions. Herein, the drift-flux model (Ishii and Hibiki 2006) is developed to a new bi-layer three-phase model describing transient mixed flows.

### 2.1 *One-dimensional bi-layer drift-flux model*

The computation of a three-dimensional (3D) multiphase model frequently requires a prohibitive computational effort such that 1D models are used if transversal velocities are negligible. 1D air–water flows can be summarized in a single model (Fig. 1b). Its stratified part is broken down into two layers. The upper layer is a pure airflow, while the lower layer is a mixture of water and dispersed air. The model includes three phases: water, dispersed air, and pure air above the free surface. In an open channel, only the lower layer with two phases appears, whereas the upper layer disappears if the free surface reaches a pipe invert.

The 3D drift-flux model simplifies by area-integration over a single flow cross-section (Fig. 1a). Using a frame of reference in which the $x$-axis is parallel to the main flow direction and the $y$- and $z$-axes are included in the cross-section. The $x$-axis is inclined by the angle $\theta$. The domain of integration contains the lower-layer free-surface width $l$, the free-surface elevation $h_s$, and the pipe bottom elevation $h_b$, so that the total height is $h = h_s + h_b$.

The integration above the lower layer gives the three partial differential equations

$$
\begin{aligned}
&\frac{\partial \langle\rho_m\rangle \Omega}{\partial t} + \frac{\partial \langle\rho_m\rangle \tilde{u}_m \Omega}{\partial x} = 0 \quad \text{(mixture continuity)}\\
&\frac{\partial \langle\alpha_d\rangle \Omega}{\partial t} + \frac{\partial}{\partial x}\left(\langle\alpha_d\rangle \tilde{u}_m \Omega + \langle\alpha_d\rangle \frac{\rho_w}{\langle\rho_m\rangle} \tilde{U}_{dj} \Omega\right)\\
&\quad = \left\langle \frac{\Gamma_d}{\rho_d} \right\rangle \Omega \quad \text{(diffusion)}\\
&\frac{\partial \langle\rho_m\rangle \tilde{u}_m \Omega}{\partial t} + \frac{\partial \langle\rho_m\rangle \tilde{u}_m \tilde{u}_m \Omega + \langle\rho_m\rangle g \cos\theta P_\Omega}{\partial x}\\
&\qquad + \frac{\partial}{\partial x}\left(\frac{\langle\alpha_d\rangle}{1-\langle\alpha_d\rangle} \frac{\rho_d \rho_w}{\langle\rho_m\rangle} \tilde{U}_{dj} \tilde{U}_{dj} \Omega\right)\\
&\quad = -\langle\rho_m\rangle g \Omega \left(\sin\theta + S_F + \frac{\partial h_b}{\partial x}\right) + \langle\rho_m\rangle \mathrm{g} \cos\theta P_{\partial\Omega}\\
&\qquad - \Omega \frac{\partial p_\Gamma}{\partial x} - S_\Gamma \quad \text{(mixture momentum)}
\end{aligned}
\tag{1}
$$

where $\Omega$ is the area of the lower layer and the bracket $\langle . \rangle$ designates the area-average of a function over $\Omega$. The mean mixture

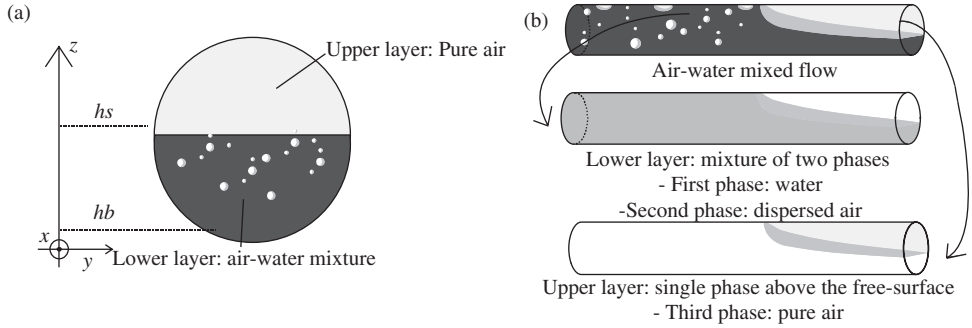


Figure 1 (a) Unified domain of integration domain, (b) original conceptual model describing all cases of air–water flows

density and mean mixture velocity are defined as

$$\langle\rho_m\rangle = \langle\alpha_d\rangle\rho_d + (1-\langle\alpha_d\rangle)\rho_w \quad \text{and} \quad \tilde{u}_m = \frac{\langle\rho_m u_m\rangle}{\langle\rho_m\rangle} \tag{2}$$

A single term depending on the area-averaged drift-velocity $U_{dj}$ governs the air diffusion in the water flow accounting for the relative velocity between both phases, defined as

$$\tilde{U}_{dj} = \langle\langle u_d\rangle\rangle - \langle j\rangle \text{ with } \langle\langle u_d\rangle\rangle = \frac{\langle\alpha_d u_d\rangle}{\langle\alpha_d\rangle} \quad \text{and}$$
$$\langle j\rangle = \langle\alpha_d\rangle\langle\langle u_d\rangle\rangle + (1-\langle\alpha_d\rangle)\langle\langle u_w\rangle\rangle \tag{3}$$

Three pressure terms appear in Eq. (1), namely the hydrostatic pressure term $P_\Omega$, the sidewall reaction to section variations $P_{\partial\Omega}$, and the pressure acting on the free-surface $p_\Gamma$ as a primitive unknown of the upper layer equations. By definition, with $\xi$ as the variable of integration

$$P_\Omega(\Omega) = \int_{-h_b}^{h_s} (h-\xi) l(x,\xi)\mathrm{d}\xi$$
$$P_{\partial\Omega}(\Omega) = \int_{-h_b}^{h_s} (h-\xi)\frac{\partial l(x,\xi)}{\partial x}\mathrm{d}\xi \tag{4}$$

The internal and external friction terms are separated into two terms, namely $S_F$ accounting for the frictional head loss in the lower layer and $S_\Gamma$ accounting for friction at the interface.

The integration of the 3D drift flux model over the upper layer (pure air) gives

$$\frac{\partial\rho_g\Omega_g}{\partial t} + \frac{\partial\rho_g\langle\langle u_g\rangle\rangle\Omega_g}{\partial x} = 0$$
$$\frac{\partial\rho_g\Omega_g\langle\langle u_g\rangle\rangle}{\partial t} + \frac{\partial\rho_g\langle\langle u_g\rangle\rangle\langle\langle u_g\rangle\rangle\Omega_g}{\partial x} + \Omega_g\frac{\partial p_\Gamma}{\partial x}$$
$$= -\rho_g \mathrm{g}\Omega_g S_g + S_\Gamma \tag{5}$$

where $\Omega_g$ is the area of the upper layer, and $\rho_g$ is air density. The pure air velocity $\langle\langle u_g\rangle\rangle$ is a primitive unknown, as also pressure $p_\Gamma$. Further $S_g$ is the frictional head loss. The upper layer equations are closed by using an equation of state defining the speed of sound in air $a_g = 330\,\mathrm{m/s}$ as

$$a_g^2 = \frac{\partial p_\Gamma}{\partial\rho_g} \tag{6}$$

### 2.2 *Extension to multiphase pressurized flows*

Equations (1)–(6) define an original 1D bi-layer model that improves the description of transient free-surface flows with air-entrainment, yet is unable to describe pressurized *and* mixed flows. The applicability of the lower layer equations is thus extended for pressurized flows by relying on shock-capturing methods (Vasconcelos and Wright 2007, Kerger *et al.* 2009). By definition, $p$ depends on the pressure wave celerity $a$ as

$$a^2 = \Omega\frac{\partial p}{\partial(\langle\rho_m\rangle\Omega)} \longrightarrow p = \int_{\langle\rho_m\rangle\Omega_{\max}}^{\langle\rho_m\rangle\Omega} \frac{a^2}{\Omega}\mathrm{d}\xi \tag{7}$$

By addition to the hydrostatic pressure term (4),

$$P_\Omega(\Omega) = \begin{cases} \displaystyle\int_{-h_b}^{h_s} (h-\xi)l(x,\xi)\mathrm{d}\xi & \text{for free surface flow} \\ P_\Omega(\Omega_{\max}, FS) + p\dfrac{\Omega_{\max}}{\langle\rho_m\rangle \mathrm{g}} & \text{for pressurized flow} \end{cases} \tag{8}$$

where $\Omega_{\max}$ is the area of the full pipe at atmospheric pressure. If $\Omega > \Omega_{\max}$, the flow is pressurized; if $\Omega \leq \Omega_{\max}$, then the flow is either pressurized or free-surface according to the aeration rate.

If celerity $a$ is considered constant in the pure water flow, its value strongly depends on the concentration in dispersed air. According to Guinot (2001),

$$a_m = \frac{a_0}{\sqrt{1+\alpha_0\rho_{m,0}a_0^2 p_0^{1/\beta}/p^{(1+\beta)/\beta}}} \tag{9}$$

where subscript 0 designates the reference state characterized by atmospheric pressure, and $\beta = 1$ for isothermal processes. By analogy with Guinot (2001), integration of Eq. (8) by using Eq. (9) for celerity gives an iterative equation for pressure $p$. Equations (8) and (9) extend the applicability of the free-surface drift-flux model to pressurized flows as well.

### 2.3 *Linear analysis*

Two-layer models as proposed here are notorious for losing their hyperbolicity under certain conditions. With $c$ as the free surface celerity, this feature is highlighted by identifying the eigenvalues $\lambda$ of the Jacobian matrix

$$\begin{cases} \lambda - \tilde{u}_m = 0 \\ \left[\lambda^2 - 2\tilde{u}_m\lambda - \left(c^2 - \tilde{u}_m^2 + a_g^2\dfrac{\rho_g}{\rho_w}\dfrac{\Omega}{\Omega_g}\right)\right] \\ \quad *[\lambda^2 - 2\langle\langle u_g\rangle\rangle\lambda - (a_g^2 - \langle\langle u_g\rangle\rangle^2)] = a_g^4\dfrac{\rho_g}{\rho_w}\dfrac{\Omega}{\Omega_g} \end{cases} \tag{10}$$

The second equation does not have any analytical solution. The numerical analysis of Eq. (10) indicates that the eigenvalues can be either real or complex, and thus the problem hyperbolic, or not. Expressing the upper layer equations in their conservative form makes the problem hyperbolic again (Audusse and Bristeau 2007). Herein, the lateral pressure term $p_\Gamma(\partial\Omega_g/\partial x)$ is neglected in the derivation of the Jacobian matrix, resulting in five real

eigenvalues

$$\lambda_1 = \tilde{u}_m; \lambda_2 = \tilde{u}_m - \sqrt{c^2 + a_g^2 \frac{\rho_g}{\rho_w} \frac{\Omega}{\Omega_g}};$$
$$\lambda_3 = \tilde{u}_m + \sqrt{c^2 + a_g^2 \frac{\rho_g}{\rho_w} \frac{\Omega}{\Omega_g}}; \lambda_4 = \langle\langle u_g \rangle\rangle + a_g;$$
$$\lambda_5 = \langle\langle u_g \rangle\rangle - a_g \tag{11}$$

Theoretically, classical explicit numerical schemes are unable to solve a non-hyperbolic problem. From a practical point of view, numerical schemes initially developed for hyperbolic problems have, however, reached a success when applied to non-hyperbolic problems if the loss of hyperbolicity originates from a small number of terms, like above. A numerical scheme was thus established for this simplified model. Its applicability is extended below to the full non-hyperbolic problem.

## 3 Numerical model WOLF IMPack

For solving the above model, the modelling system WOLF that was developed at the University of Liège is employed. Its validity was verified by Dewals *et al.* (2006), and Erpicum *et al.* (2009). The implementation of the above equations into WOLF results into the new computational module WOLF IMPack (Integrated Multi-Phase Pack).

WOLF IMPack relies on a finite volume discretization and a flux vector splitting (FVS). Herein, the 1D bi-layer three-phase system is solved over a uniform grid containing cells of length $\Delta x_i = x_{i+1/2} - x_{i-1/2}$, $i = 1, N$ (Fig. 2). The explicit updating formula is given by

$$\boldsymbol{U}_i^{n+1} = \boldsymbol{U}_i^n - \frac{\Delta t}{\Delta x_i}[F_{i+1/2}(\boldsymbol{U}^n) - F_{i-1/2}(\boldsymbol{U}^n)] - \frac{\Delta t}{\Delta x_i} P_i(\boldsymbol{U}^n) + \Delta t \boldsymbol{S}_i^n$$
$$\boldsymbol{U}_i = [\{\langle\rho_m\rangle\Omega\}_i \quad \{\langle\alpha_d\rangle\Omega\}_i \quad \{\langle\rho_m\rangle\tilde{u}_m\Omega\}_i \quad \{\rho_g\Omega_g\}_i \quad \{\rho_g\langle\langle u_g\rangle\rangle\Omega_g\}_i]^T \tag{12}$$

where $i$ is the spatial index, $n$ the time index, and $\Delta t$ the time step of the temporal integration. To prevent post-transition numerical oscillations, the numerical filtering approach proposed by Vasconcelos *et al.* (2009) was implemented with values of $\varepsilon$ between 0.0005 and 0.025

$$\boldsymbol{U}_i^{n+1} = (1 - 2\varepsilon)\boldsymbol{U}_i^{n+1} + \varepsilon(\boldsymbol{U}_{i-1}^{n+1} + \boldsymbol{U}_{i+1}^{n+1}) \tag{13}$$

The conservative numerical flux $\mathbf{F}_{i+1/2}$ is computed with an FVS originally proposed for shallow-water equations (Dewals *et al.* 2006, Erpicum *et al.* 2009) as

$$\boldsymbol{F}_{i+1/2} = \begin{bmatrix} \{\langle\rho_m\rangle\tilde{u}_m\Omega\}_{i+1/2}^L & \{\langle\alpha_d\rangle\tilde{u}_m\Omega\}_{i+1/2}^L \\ \{\rho_g\langle\langle u_g\rangle\rangle\Omega_g\}_{i+1/2}^L & \\ \{\langle\rho_m\rangle\tilde{u}_m\tilde{u}_m\Omega\}_{i+1/2}^L + \{\langle\rho_m\rangle \mathrm{g}\cos\theta P_\Omega\}_{i+1/2}^R & \\ \{\rho_g\langle\langle u_g\rangle\rangle\langle\langle u_g\rangle\rangle\Omega_g\}_{i+1/2}^L & \end{bmatrix}^T \tag{14}$$

where $L$ designates the up- and $R$ the downstream reconstructed values (Fig. 2). The two sides are determined by analysing the sign of the mixture velocity $\tilde{u}_m$ for the first three equations describing the lower layer, and the sign of the gas phase velocity $\langle\langle u_g\rangle\rangle$ for the last two equations describing the upper layer. The non-conservative numerical flux $\boldsymbol{P}_i$ is

$$\boldsymbol{P}_i = \begin{bmatrix} 0 \\ 0 \\ [(\{\Omega\}_{i-1/2}^R + \{\Omega\}_{i+1/2}^R)/2] * [(\{p_\Gamma\}_{i+1/2}^R - \{p_\Gamma\}_{i-1/2}^R) \\ \quad + \langle\rho_m\rangle \mathrm{g}(\{h_b\}_{i+1/2}^R - \{h_b\}_{i-1/2}^R)] \\ 0 \\ 0.5(\{\Omega_g\}_{i-12}^R + \{\Omega_g\}_{i+1/2}^R)(\{p_\Gamma\}_{i+1/2}^R - \{p_\Gamma\}_{i-1/2}^R) \end{bmatrix} \tag{15}$$

All other terms are included in the centered source term $\boldsymbol{S}_i$. Consistence, order of accuracy and stability of the method has been extensively studied. The stability of the scheme is ensured under the conditions of the Courant–Friedrichs–Levy (CFL) criterion. The CFL number is computed using the maximum wave velocity and the approximate eigenvalues of Eq. (11) as

$$\mathrm{CFL} = \max_{i=1,5}(|\lambda_i|)\Delta x/\Delta t \tag{16}$$

Constant reconstruction gives a first order of accuracy in a uniform grid. The linear reconstruction increases the accuracy of one order. For a two-phase water hammer (Section 4.2), a convergence study is performed. Figure 3 shows the evolution of the error computed on 25 points along the pipe as

$$\log_{10}\varepsilon = \log_{10}\sqrt{\frac{\sum_{i=1,25}(P_i^N - P_i^{ref})^2}{25}} \tag{17}$$

where the reference state includes 1200 meshes. As expected, this error uniformly decreases with respect to the number of meshes $N$.

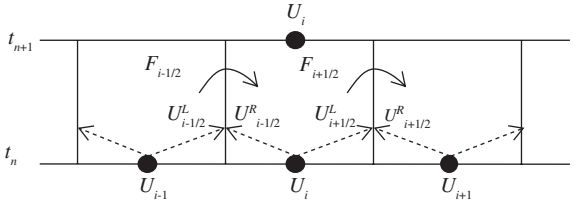


Figure 2 Finite volume method

## 4 Validation and application

WOLF IMPack was assessed by a large programme of validation (Kerger 2010). Analytical, numerical, and experimental

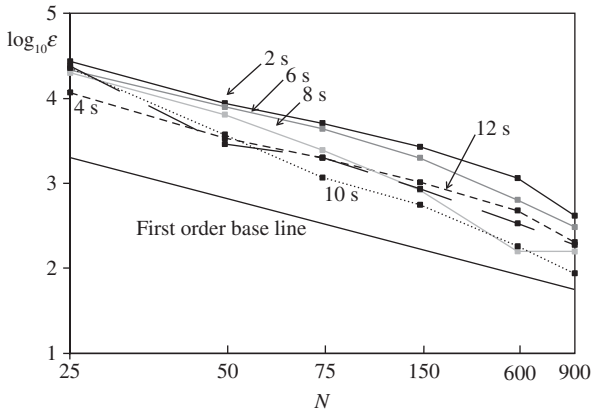


Figure 3 Error $\log_{10} \varepsilon$ versus number of meshes $N$ for two phase water

benchmarks included pressurized flows, free surface flows of sub-, super-, and transcritical regimes, and mixed flows. Both pure water flows and air–water interactions were considered. Furthermore, the new code underpinned the design of actual hydraulic structures like a gravity drainage system, a low pressure sewer system (Kerger *et al.* 2009), and the bottom outlet of a dam (Kerger *et al.* 2011). Here the results of the most evocative cases are presented.

### 4.1 *Mixed flows: rapid pipe filling*

The ability of WOLF IMPack to simulate mixed flows is compared with a classical benchmark: rapid pipe filling (Vasconcelos *et al.* 2009). The study was conducted on an experimental set-up described by (Vasconcelos and Wright 2005). It consists of a 14.3 m long, 94 mm diameter acrylic pipeline, connected at the upstream end to an inflow box of lateral dimensions 0.25 m × 0.25 m, and at the downstream end with a surge riser of 0.19 m diameter. The pipeline was initially filled with 7.3 cm of stagnant water. A constant inflow of 3.1 l/s was suddenly added to the fill box, which immediately formed a pipe-filling bore front propagating towards the surge riser.

The computations were performed on a uniform grid of 791 meshes 0.019 m long. Both the up- and downstream tanks were simulated such that the boundary conditions represent impermeable walls. Using a two-step Runge-Kutta RK31 time integration, the computational time was 400 s for 40 s of simulation on a PC. The CFL number was kept constant at 0.3 and the filter constant at 0.025. The computational results are compared with the experimental data in Fig. 4. Adequacy is obvious between both "mean" curves at each measurement stations. A numerical filter prevents spurious oscillations at the transition bore but keeps physical oscillations linked to the water hammer (Fig. 4a).

### 4.2 *Air-entrainment: two-phase water hammer*

This standard benchmark is presented by Guinot (2001), consisting of a 3000 m long circular pipe of area 0.29 $m^2$. The reference celerity is 981 m/s while the reference density is 992 $kg/m^3$. The void fraction is assumed constant at 0.2%. The fluid is initially at rest, at a pressure of $5 \times 10^5$ Pa. At time $t = 0$, the pressure at the left-hand boundary is lowered to $10^5$ Pa, causing a rarefaction wave to travel to the right. Upon reflection at the pipe end, a shock wave occurs. This feature is critic for air-entrainment and has never been simulated by any mixed flows codes.

The numerical computation was performed on a uniform grid of 300 cells each 10 m long. Time integration was performed

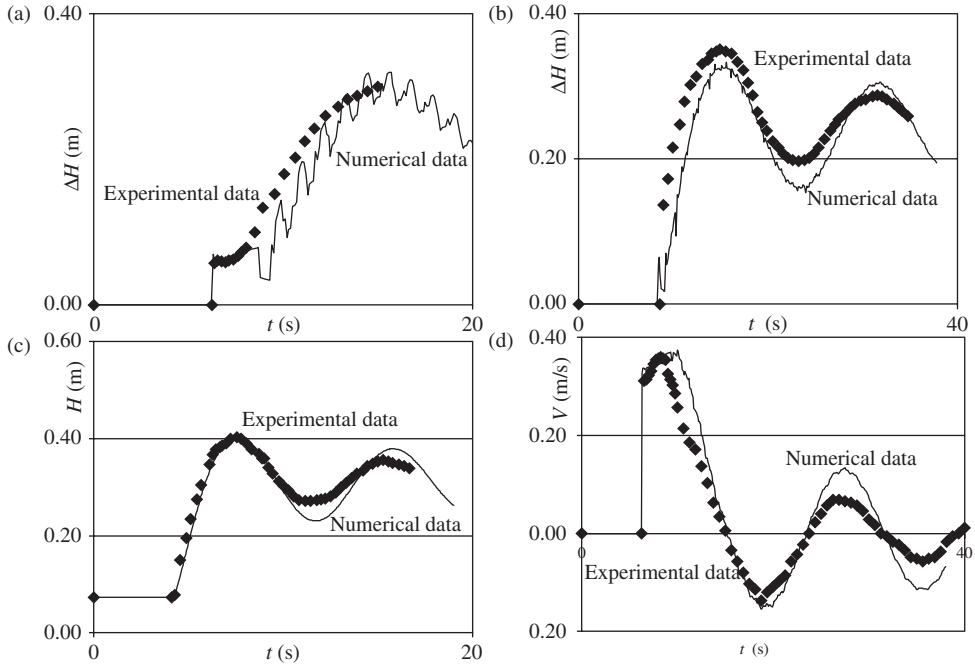


Figure 4 Comparison between experimental data (Vasconcelos *et al.* 2006) with numerical data from WOLF IMPack. Pressure head-time evolution from filling box (a) 9.9 m, (b) 14.1 m, (c) pressure head-time evolution in surge riser, (d) velocity-time evolution 9.9 m from filling box

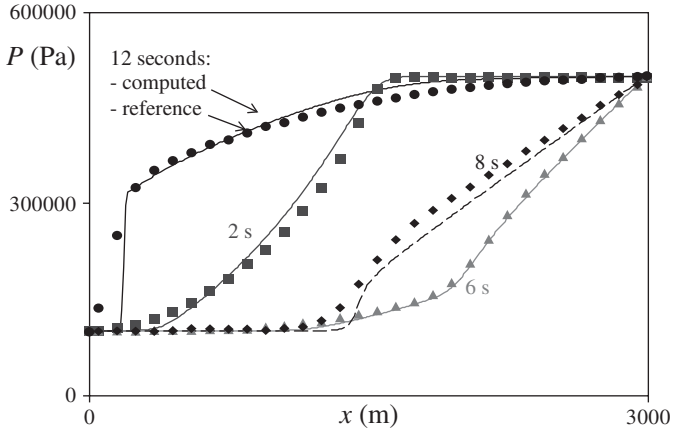


Figure 5 Comparison between data of Guinot (2001) and results given by WOLF IMPack for pressure profile $P(x)$

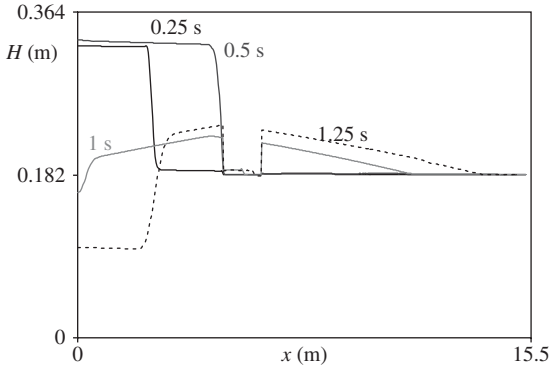


Figure 7 Pressure head profiles $H(x)$ at different times underlining water tank effect

with a three-step Runge–Kutta scheme (RK31) with the CFL number kept at 0.4. The computation took 6.72 s for a 12 s simulation on a PC. Figure 5 compares the pressure profiles computed at 2, 6, 8, and 12 s with WOLF IMPack with these of Guinot (2001), resulting from a two-phase water hammer code. Contrary to a single phase water hammer characterized by a sharp shock wave translating at constant velocity, a rarefaction wave occurs due to the relation between pressure and celerity. The wave is reflected at the right-hand pipe side and the resulting wave steepens when travelling to the left hand-side. This water hammer is thus strongly non-linear. The lower the pressure, the lower is the celerity. Results from WOLF IMPack agree well with the data of Guinot (2001).

### 4.3 *Closed surge tanks dynamics*

Closed surge tanks constitute an interesting benchmark for WOLF IMPack, because it gives insight into their hydraulic features. The benchmark considers a circular pipe of 0.094 m diameter. A closed surge tank was placed 5 m downstream from the pipe entrance. The tank was 1.25 m long, 0.25 m wide and 1 m high. Beyond the tank, a pipe 0.094 m wide and 9.05 m long was connected to a device keeping the pressure constant at 0.1825 m. The water was initially at rest with a pressure of 0.1825 m. The approach flow discharge was suddenly increased to 0.001 $m^3/s$ so that a water hammer resulted (Fig. 6).

The numerical computation was performed on a uniform grid of 100 cells each 0.025 m long. Time integration was performed again with a RK31 scheme and CFL = 0.4, which took 1000 s for a 1.5 s simulation on a PC. As shown in Fig. 7, the sudden discharge increase creates a pressure surge propagating at pressure wave celerity within the pipe. After 0.5 s, the water hammer impacts the surge tank. The free surface level in the tank slowly increases. Next, the elevation of the free surface level induces a pressure increase in the downstream pipe, yet which is much smaller than the increase upstream. While a high-intensity water hammer propagates between the upstream end and the tank, a smaller wave travels between the tank and the downstream pipe end. The tank efficiency is explained by both the small celerity of free surface flows and the cushion effect of entrapped air, described adequately by WOLF IMPack.

### 4.4 *Air-entrapment: moving mixed flows*

One of the objectives of IMPack is to describe the entrapment of air pockets by mixed flow. Consequently, WOLF IMPack was applied on two benchmarks involving mobile transitions and active upper layers: the entrapment of air bubbles at high points of pipelines and the rapid pipe filling. However, post-transition oscillations occur in the lower layer contaminating the upper layer. Since the air pressure celerity is large at 330 m/s, these oscillations rapidly reduce the numerical stability. Even the numerical filter of Vasconcelos *et al.* (2009) was insufficient to

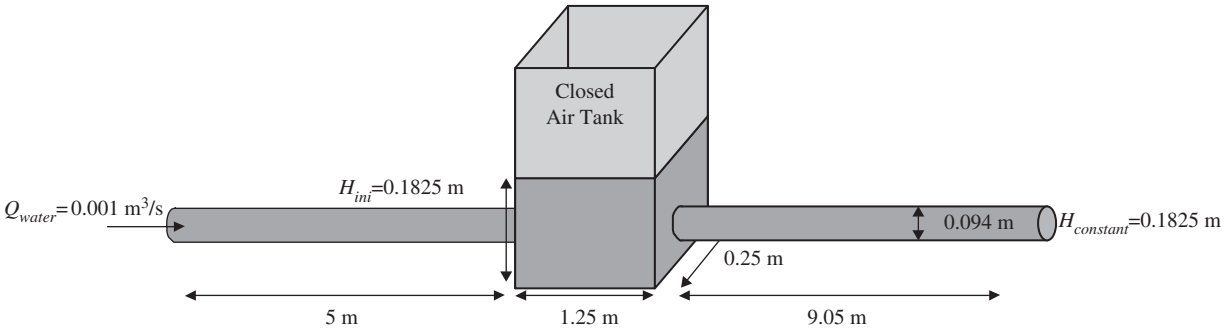


Figure 6 The benchmark exemplifies the functioning principle of a closed surge tank located in the middle of a circular pipe

prevent the problem. This observation indicates that numerical shock-capturing methods are partly inefficient in the presence of highly variable celerities, a shortcoming linked to the discretization of both the equations and the computational domain (Vasconcelos *et al.* 2009). Kerger (2010) and Kerger *et al.* (2011a) proved that any numerical shock-capturing solver is affected by this flaw.

## 5 Conclusions

This research presents a new multiphase mathematical model describing transient air water mixed flows. Based on the drift-flux model, the original set of equations developed governs the evolution of three phases in two layers. The upper layer contains only air while the lower layer includes both water and dispersed air phases. The pressure gradient in the lower layer was modified to extend the model applicability to two-phase pressurized flows. This new term accounts for the effect of dispersed air on the pressure wave celerity. The set of governing five partial differential equations was discretized, using the finite volume method and implemented into WOLF IMPack. These innovations are validated with benchmarks, and then the code was applied to various cases of engineering interest presented in a companion paper.

The new code enables to simulate open channel flow, mixed flows and water hammers in a unified framework. The multiphase approach accounts for air-entrainment in these three flows and air-entrapment in closed pipes. The code is able to handle non-uniform pipe sections and variable pressure wave celerities as a function of void fraction. This study also includes one limitation of shock-capturing approaches: post-transition oscillations produced by the numerical scheme, even with a numerical filter, do not allow for simulating air-entrapment by a moving transition, whereas air-entrapment by a fixed transition is correctly retained. This shortcoming is a challenge, paving the way to further research on air–water mixed flows.



## Notation

$c, a$ = free surface and pressure wave celerity ($ms^{-1}$)
$F, S$ = flux and source term (–)
g = gravitational constant ($ms^{-2}$)
$h$ = height (m)
$i, n$ = space and time index (–)
$j$ = volumetric flux ($ms^{-1}$)
$l, L$ = free surface width (m)
$L, R$ = left and right (–)
$M$ = mixture momentum source ($kg\,m^{-2}s^{-2}$) or density function (–)
$P, p$ = area-integrated pressure (N) and pressure ($Nm^{-2}$)
$S$ = head loss slope (–)
$t$ = time (s)
$x, y, z$ = space variables (m)
$v, V, u, U$ = velocity ($ms^{-1}$)

*Greek letters*

$\alpha$ = void fraction (–)
$\beta$ = adiabatic or isothermal coefficient (–)
$\Delta$ = local gradient (–)
$\varepsilon$ = relative error, filtering constant (–)
$\Gamma$ = mass source term ($kg\,m^{-3}s^{-1}$)
$\theta$ = angle between $x$-axis and horizontal (–)
$\xi$ = variable of length integration (m)
$\rho$ = density ($kg\,m^{-3}$)
$\tau$ = stress ($Nm^{-2}$)
$\Omega$ = area ($m^2$)

*Subscripts and exponents*

0 = reference state
$d, w$ = dispersed air and water phases
$F$ = friction
$g$ = upper layer
$j$ = drift value
$m$ = mixture of water and air
max = max maximum
$s, b$ = free surface, bottom
$Sat$ = saturation state in air
$T, D$ = turbulent and diffusion
$\Gamma$ = interface

## References


Audusse, E., Bristeau, M.-O. (2007). Finite-Volume solvers for a multilayer Saint-Venant System. *Int. J. Applied Math. Computer Science* 17(3), 311–320.

Bourdarias, C., Gerbi, S. (2008). A conservative model for unsteady flows in deformable closed pipes and its implicit second order Finite Volume discretisation. *Computers & Fluids* 37(10), 1225–1237.

Bourdarias, C., Gerbi, S., Gisclon, M. (2008). A kinetic formulation for a model coupling free surface and pressurized flows in closed pipes. *J. Comp. Applied Mathematics* 218(2), 522–532.

Dewals, B.J., Erpicum, S., Archambeau, P., Detrembleur, S., Pirotton, M. (2006). Depth-integrated flow modelling taking into account bottom curvature. *J. Hydraulic Res.* 44(6), 787–795.

Erpicum, S., Dewals, B.J., Archambeau, P., Pirotton, M. (2009). Dam-break flow computation based on an efficient flux-vector splitting. *J. Comput. Appl. Math.* 234(7) 2143–2151.

Guinot, V. (2001). Numerical simulation of two-phase flow in pipes using Godunov method. *Int. J. Numerical Methods Eng.* 50(5), 1169–1189.

Guo, Q., Song, C. (1990). Surging in urban storm drainage systems. *J. Hydraulic Eng.* 116(12), 1523–1537.

Guo, Q., Song, C. (1991). Dropshaft hydrodynamics under transient conditions. *J. Hydraulic Eng.* 117(8), 1042–1055.

Ishii, M., Hibiki, T. (2006). *Thermo-fluid dynamics of two-phase flow*. Springer Science, New York.

Jha, S., Bombardelli, F. (2009). Two-phase modeling of turbulence in dilute sediment-laden, open-channel flows. *Env. Fluid Mech.* 9(2), 237–266.

Kerger, F. (2010). Modelling transient air-water flows in civil and environmental engineering. *PhD Thesis*. ArGEnCo, University of Liège, Liège.

Kerger, F., Archambeau, P., Erpicum, S., Dewals, P., Pirotton, M. (2009). Simulation numérique des écoulements mixtes hautement transitoire dans les conduites d'évacuation des eaux. *La Houille Blanche* 64(5), 159–167 [in French].

Kerger, F., Archambeau, P. , Erpicum, S., Dewals, P., Pirotton, M. (2011a). An exact Riemann solver and a Godunov scheme for simulating highly transient mixed flows. *J. Comp. Applied Mathematics* 235(8), 2030–2040.

Kerger, F., Archambeau, P. , Erpicum, S., Dewals, P., Pirotton, M. (2011b). 1D unified mathematical model for environmental flow applied to steady aerated mixed flows. *Adv. Eng. Software* 42(9), 660–670.

Leon, A., Ghidaoui, M.S., Schmidt, A.R., Garcia, M.H. (2008). Application of Godunov-type schemes to transient mixed flows. *J. Hydraulic Res.* 47(2), 147–156.

Leon, A., Ghidaoui, M.S., Schmidt, A.R., Garcia, M.H. (2010). A robust two-equation model for transient-mixed flows. *J. Hydraulic Res.* 48(1), 44–56.

Li, J., McCorquodale, A. (1999). Modeling mixed flow in storm sewers. *J. Hydraulic Eng.* 125(11), 1170–1180.

Politano, M., Odgaard, A.J., Klecan, W. (2007). Numerical evaluation of hydraulic transients in a combined sewer overflow tunnel system. *J. Hydraulic Res.* 133(10), 1103–1110.

Shu, J.-J. (2003). Modelling vaporous cavitation on fluid transients. *Int. J. Pressure Vessels & Piping* 80(3), 187–195.

Vasconcelos, J., Wright, S. (2005). Experimental investigation of surges in a stormwater storage tunnel. *J. Hydraulic Eng.* 131(10), 853–861.

Vasconcelos, J.G., Wright, S.J., Roe, P.L. (2006). Improved simulation of flow regime transition in sewers: The two-component pressure approach. *J. Hydraulic Eng.* 132(6), 553–562.

Vasconcelos, J.G., Wright, S.J. (2007). Comparison between the two-component pressure approach and current transient flow solvers. *J. Hydraulic Res.* 45(2), 178–187.

Vasconcelos, J.G., Wright, S.J. (2009). Investigation of rapid filling of poorly ventilated stormwater storage tunnels. *J. Hydraulic Res.* 47(5), 547–558.

Vasconcelos, J.G., Wright, S.J., Roe, P.L. (2009). Numerical oscillations in pipe-filling bore predictions by shock-capturing models. *J. Hydraulic Eng.* 135(4), 296–305.

Zhou, F., Hicks, F.E., Steffler, P.M. (2002). Transient flow in a rapidly filling horizontal pipe containing trapped air. *J. Hydraulic Eng.* 128(6), 625–634.